Reduced Interfacial Adhesion in Glass Fibre-Epoxy Composites due to Water Absorption via Molecular Dynamics Simulations

Mark T. Stoffels[a], Mark P. Staiger[a], Catherine M. Bishop[a,*]

[a] *Department of Mechanical Engineering, University of Canterbury, Private Bag 4800, Christchurch, 8140 New Zealand*

Abstract

Molecular Dynamics simulations were used to investigate the effects of absorbed water on interfacial adhesion in an epoxy glass composite. The composite comprised SiO_2 fibres, γ-Aminopropyltriethoxysilane (AMPTES) fibre sizing, and a diglycidyl ether bisphenol A (DGEBA)/isophorone diamine (IPD) epoxy matrix. An average solubility limit of 2.07 wt.% water was found in the simulated system, equivalent to 0.99 wt.% water in a full composite, while an experimental value of 1.15 wt.% was determined. The work of adhesion was calculated for simulated composites and compared to experimental tensile strength in unidirectional composites. Results for both dry and saturated conditions indicated SiO_2-sizing as the critical interface for failure. Scanning electron microscopy of failed composites suggests more cohesive failures in the epoxy for the dry samples, while relatively clean fibre surfaces in the saturated samples indicate adhesive failure at the interface. This study shows how molecular simulation can be applied to sized fibre-reinforced composites.

Keywords: Fibre/matrix bond, Environmental degradation, Polymer-matrix composites, Computational modelling

*Principal corresponding author
Email address: catherine.bishop@canterbury.ac.nz (Catherine M. Bishop)

1. Introduction

Exposure to environmental conditions proves to be a primary consideration for many designs based on advanced fibre-reinforced polymer matrix composites (FRPs), notably where the materials will be operating in moisture-rich environments (*e.g.* marine environments). FRPs will normally absorb water during long-term exposure [1]. Moreover, such composite systems may experience a drastic loss in mechanical properties due to water uptake [2, 3]. In general, water absorption in polymeric composites tends to increase the ductility and flexibility, while decreasing elastic modulus and strength.

The strength of FRPs is highly dependent on fibre-matrix interfacial adhesion and the ability of the interface to transfer stress from the matrix to the reinforcing phase. The importance of the interface on the mechanical properties of FRPs has driven much research effort into understanding, controlling, and modification of the interfacial region. The direct examination of the fibre-matrix interface (and associated interphases) in FRPs is inherently complicated due to structures that range from the microscopic down to the molecular scale. Consequently, the specific adhesion mechanisms and associated interactions that occur at the fibre-matrix interface are not fully understood due to the difficulty in experimentally probing the structure.

Studies have used fluorescence [4], FTIR [5, 6], NMR [7], and Raman [8, 9] spectroscopic techniques as means of probing the interface, but results are inconclusive and often conflicting. Furthermore, few studies have found success in considering the specific effects of water on interfacial adhesion. Overall, the underlying mechanisms for the loss of interfacial adhesion in FRPs due to the presence of absorbed water are not well understood due to experimental difficulties involved with probing structural changes at the fibre-matrix interface.

Recently, Molecular Dynamics (MD) simulation has proven to be a powerful tool for investigating molecular level interactions in polymeric systems [10–12]. Clancy and Mattice investigated the interface between polymer-polymer systems using MD methods [13]. Simulation procedures were presented for the generation of bulk and slab structures, and for the calculation of surface energy and work of adhesion. Surface energy, γ, quantifies the amount of energy required to form a unit area of new surface,

$$\gamma = \frac{U_{slab} - U_{bulk}}{2A} \tag{1}$$

where, U_{slab} and U_{bulk} are the potential energies for the slab and bulk material, while A is the projected surface area. Fundamentally, the work of adhesion, W_{12}, is the amount of work required to separate

two adjacent phases 1 and 2,

$$W_{12} = \frac{U_{slab,1} + U_{slab,2} - U_{12}}{2A} \tag{2}$$

where, $U_{slab,1}$ and $U_{slab,2}$ are the potential energies for slab materials 1 and 2 and U_{12} is the potential energy for the entire, combined system. These methods were expanded on for use with SiO_2-epoxy [14] and polymer-silane [15] interfaces.

Coating fibres with a sizing is an essential manufacturing step in most commercial fibre composite systems and is critically important as it promotes fibre-matrix adhesion at the molecular level. Proprietary interests often obscure the precise composition and application of many commercial sizing formulations. The amount of sizing applied to a glass fibre surface is reported as a wt.% and varies between 0.2 to 1.0 wt.%. Of this, approximately 10 - 20% is assumed to be a strongly bounded silane component, while the remaining 80 - 90% constitutes film formers and other additives [16]. Successful implementation of MD requires a well developed understanding of initial atomic structures and relative molecular arrangements. Specifics on fibre sizing are ambiguous, where the precise amount and exact composition at any given portion of the fibre is generally not known. While MD methods used in determining surface energies and work of adhesion at an interface are well understood, studies on the applications of MD to examining adhesion at fully sized interfaces in fibre reinforced polymer composites are lacking.

In the present work, a slab composite consisting of glass fibre, silane sizing layer, and polymer matrix is investigated using MD simulation. The silane coupling agent γ-Aminopropyltriethoxysilane (AMPTES) was selected as fibre sizing, while an epoxy system consisting of diglycidyl ether bisphenol A (DGEBA) using isophorone diamine (IPD) as the curing agent was selected. These were chosen due to their common use throughout industry. Novel methods for (*i*) generating representative slab composite interface simulation cells and (*ii*) saturating the slab composite interface with water are proposed. The work of adhesion is calculated for replicates of dry, moist, and fully saturated slab composites and compared to experimental tensile strength in equivalent, unidirectional composites. Importantly, this MD study is novel in that it considers the sizing as part of the molecular description of the fibre-matrix interface, specifically addressing an area lacking in literature.

2. Methods

2.1. Molecular Dynamics Simulations

The LAMMPS package was used for all MD simulations [17]. The Nosé-Hoover thermostat and Berendsen barostat were employed [18, 19]. Unless otherwise specified, all simulations were carried out at a pressure of 1 atm and temperature of 300 K, with fully periodic boundary conditions. A modified Born-Mayer-Huggins (BMH) potential was used to describe all pairwise interactions of atoms in the SiO_2 structure [20], while a modified Stillinger-Weber (SW) potential captured all three body interactions [21]. The CHARMM force field was employed in defining the bond, angle, and dihedral parameters for all sizing and epoxy atoms [22]. A cutoff distance of 10 Å was used to calculate contributions per atom to the potential energy and net forces. MD ensembles were enacted at various times to thermodynamically constrain the system: (*i*) NVT - constant number of atoms, volume, and temperature and (*ii*) NPT - constant number of atoms, pressure, and temperature. The procedure for making composites described next was replicated ten times to generate ten thermodynamically equivalent slab composite systems.

2.1.1. The Slab Composite

A melt-quench procedure was used to simulate the amorphous SiO_2 (a-SiO_2) structure [20, 23]. A 2880 atom crystalline α-quartz SiO_2 structure was used as the starting configuration, resulting in a simulation box size of 42.80 Å × 42.80 Å × 19.73 Å. The system was melted at 5000 K and equilibrated for 20 ps of NVT. Then, the structure was quenched to 300 K at a constant rate over 200 ps under NPT. Finally, the system was equilibrated for 50 ps of NVT. A glass fibre surface was created from the a-SiO_2 structure by immobilising the bottom 720 atoms and removing the periodic boundary in the z-direction. 50 ps of NVT dynamics were run to equilibrate.

For the purposes of this work only the strongly bound silane coupling agent portion of the sizing was included. The total unit mass for a complete fibre diameter was calculated to determine the number of AMPTES molecules to include, where it was assumed that 0.2 wt.% represents the total mass of silane on the fibre (20% of the assumed 1.0 wt.% sizing applied). Assuming a typical fibre diameter of 10 µm, [24] a total of 146 AMPTES molecules equates to 0.2 wt.% silane sizing on the simulated fibre surface. 146 AMTPES molecules were placed adjacent to the fibre surface: the rotation and orientation of each molecule was constrained, using Packmol [25], such that the functional silane group was perpendicular to the a-SiO_2 surface. The packing tolerance was specified as 2 Å. The bottommost

720 atoms of the SiO_2 were immobilised and the periodic boundary removed in the z-direction. The system was equilibrated with 50 ps of NVT. At this point, the simulation cell dimensions were 43.20 Å $\times$ 43.85 Å $\times$ 32.01 Å.

256 reactive DGEBA and 128 reactive IPD molecules were packed above the existing sized glass fibre cell to a thickness of 100 Å, chosen to give approximately the correct density found in our previous work [10]. The packing tolerance was specified as 2 Å. Initially, 50 ps of NVT dynamics were run as before. The relaxed epoxy structure was then dynamically crosslinked under an NVT ensemble, following our previous work [10]. The DGEBA-IPD system obtained a 91.5% crosslink density.

All epoxy molecules within 15 Å of the top epoxy surface and the bottommost 720 atoms of the SiO_2 atoms were immobilised. This effectively simulates a semi-infinite slab composite where there exists bulk a-SiO_2 at one end of the cell and a bulk crosslinked DGEBA-IPD epoxy network at the other, Fig. 1. The full slab interface was further equilibrated under an NVT ensemble. After every 10 ps, a time-averaged potential energy value over the previous 10 ps was calculated. The system was considered equilibrated when the difference in system potential energy was less than 0.5% from the previous time-averaging, or after 200 ps of total simulation time. While the NPT ensemble is appropriate for simulating equilibrium density of cured epoxies, the broken symmetry of the slab complicates its use here [26]. The complete, relaxed simulation cell dimensions were 44.78 Å $\times$ 45.05 Å $\times$ 132.71 Å.

2.1.2. Saturating the Slab Composite

Determining when the composite interface is saturated with water is complicated by the inhomogeneous nature of the system. In our previous work a hybrid particle insertion/thermodynamic integration method was used to determine the solubility limit of water in bulk DGEBA-IPD, where noble water molecules were used in place of full water for the insertion process. Noble water has Coulombic interactions deactivated, Lennard-Jones interactions of the hydrogen atoms switched off, and oxygen atoms scaled to 80% of their original size. This scaling leads to a much higher success rate of particle insertions, greatly decreasing computational time [10]. In the current work, Grand Canonical Monte Carlo (GCMC) exchanges of noble water molecules were performed. After saturation, all noble water molecules were scaled back to full TIP3P water interactions [27].

For each exchange, coordinates and orientation were randomly generated, the total potential energy for the system was calculated, and the Metropolis criterion was used in determining whether or not to accept the proposed GCMC move [28]. The system was deemed to have reached saturation when no

further insertions were possible.

To undertake GCMC exchanges, it was necessary to designate the temperature and chemical potential for the exchange reservoir. The chemical potential for noble water was calculated [29], where 30 configurations of a 500 molecule noble water system were considered. An average chemical potential of -14.86 kJ mol^{-1} was found for noble water at 300 K and 1 atm. GCMC exchanges were then undertaken in the epoxy and sizing. All noble water molecules were scaled back to the full TIP3P water model using ten equidistant scaling steps, where each step was equilibrated for 20 ps of NPT.

2.1.3. Surface Energy and Work of Adhesion

The bulk structures for the a-SiO_2, AMPTES sizing, and DGEBA-IPD epoxy were extracted from the slab composite interface (Fig. 1). Slab structures were created by extending the size of the periodic simulation box of the bulk material in the $\pm z$-directions by 50 Å and padding with vacuum. The resulting cell becomes representative of a semi-infinite slab surface. Next, the slab surfaces were subjected to 100 ps of NVT, and the trajectory was saved every 0.5 ps over the final 20 ps. The trajectory with the lowest total potential energy was further minimised in order to create the final slab surface. Surface energy for each phase was then calculated, Eqn. (1).

The work of adhesion was calculated for (*i*) fibre-sizing and (*ii*) sizing-epoxy interfaces, (Supplemental Fig. 1). The SiO_2-epoxy (unsized) interface was considered for comparison. The potential energy for the slab composite U_{12} was considered as a time-averaged value over 20 ps of simulation. The two instances of interface separation were then considered, each requiring the creation of two slab surfaces. Therefore, four slabs were created: SiO_2, sizing-epoxy, epoxy, and SiO_2-sizing. The slabs were created and potential energy calculated as for the full slab composite. Work of adhesion was then calculated from Eqn. (2).

2.2. Experimental Methods

Unidirectional $[0]_4$ glass fibre [Saertex U14EU920]-epoxy laminates were fabricated using vacuum-assisted resin transfer moulding (VARTM) method. The epoxy DGEBA-IPD [Sigma-Aldrich] was allowed to cure for 24 hours at room temperature, and was then post cured for 2 hours at 160 °C. Ten samples were cut perpendicular to the fibre direction and were polished to 0.6 μm using a Buehler MicroCloth and diamond suspension. Microstructural image analysis was performed and an average fibre volume fraction of 56.3 ± 2.5% was found.

Tensile testing was conducted in accordance with ASTM D3039 [30]. 20 individual tensile testing coupons were cut from the unidirectional composite to dimensions of 200 × 15 mm ($L \times w$). Half of the samples were placed in distilled water at room temperature. Samples were removed episodically from the water bath, patted dry with a paper towel and left on the lab bench for surface water to evaporate before being weighted on a balance with ±0.1 µg precision. Full saturation was obtained when mass gains plateaued. Tensile testing was done using a 10 kN load cell at a constant crosshead speed of 1 mm/min, axial strain was recorded *via* an MTS Fundamental Video Extensometer. Friction tabs were used to mitigate gripping damage to the specimens.

Fracture surfaces were examined with a JEOL JSM IT-300 variable pressure scanning electron microscope (SEM) equipped with an Oxford Aztec SDD energy dispersive spectrometer (EDS). SEM specimens were sputter-coated with carbon and imaged at an accelerating voltage of 5 kV.

3. Results and Discussion

3.1. Amorphous SiO_2

For one generated a-SiO_2 structure an average final density of 2.274 ± 0.077 g cm^{-3} was obtained, in good agreement with reported experimental densities in the range of 2.15 - 2.29 g cm^{-3} [31]. The Radial Distribution Functions (RDF) for all atom pairs in the a-SiO_2 system was calculated as a time-averaged value over the final 1 ps of the simulation. The generated structure is in good agreement with experimental RDF values [23], Supplemental Fig. 2.

3.2. Saturation

Using the GCMC insertion process, an average of 244 water molecules were successfully inserted into each slab composite, corresponding to 2.07 wt.% water. The water content by weight was calculated from the top surface of the epoxy using a moving 5 Å window for the ten simulated composite slab structures (Fig. 2). The epoxy shows a solubility limit of 3.35 ± 0.23 wt.%, consistent with a simulated solubility limit for bulk DGEBA/IPD in the range of 3.50 - 3.75 wt.% water found in our previous work [10]. This validates the saturation procedure used here, where polar interactions with the epoxy are initially ignored during GCMC exchanges of noble water before relaxation with the full potential. These polar interactions are expected to be important given the strong polarization of cross-linked epoxy structures [26, 32]. The sizing shows a distinct increase in solubility limit with an average of 5.35 ± 0.33 wt.%. The above result suggests that there tends to be a preference for water molecules

to absorb closer to the fibre surface, in agreement with experimental studies [4, 7]. This could be attributed, in part, to the comparatively lower density of the sizing.

Fibre volume fraction (V_f) was not taken into account when generating the simulated interface system, as a result, the simulated maximum water content is not comparable with experimental values. The solubility limit M_c (wt.% water) for a equivalent full composite was calculated,

$$M_c = \frac{\rho_e V_e M_e + \rho_s V_s M_s + \rho_f V_f M_f}{\rho_e V_e + \rho_s V_s + \rho_f V_f} \tag{3}$$

where the subscripts e, s, and f represent the epoxy, sizing, and fibre, and V is the volume, ρ the saturated density, and M is the solubility limit in wt.% water. M_e is taken as 3.35 wt.% and M_s as 5.35 wt.% (Fig. 2) and glass fibre is assumed impermeable, such that $M_f = 0$. The experimental volume fraction of fibres $V_f = 56\%$, an average fibre diameter of 10 μm, and a 10 Å thick sizing layer were used. Equation (3) gives the solubility limit for the full composite $M_c = 0.99$ wt.%. The average experimental solubility limit for the unidirectional $[0]_4$ samples was 1.15 $\pm$ 0.02 wt.%, indicating the simulated system underestimates the maximum water content by 13.7%.

The simulated interface used a sizing thickness of 10 Å, while in reality this thickness will be far greater. An estimate for the sizing thickness was made through iterative applications of Eqn. (3). Using this method, an estimated sizing thickness of 147.3 nm was found. This falls in the range reported for silane sizings, 1 nm - 1 μm [33, 34].

3.3. Adhesion at the Interface

Table 1 and Fig. 3 provide summaries of the calculated surface energies. Results show that SiO_2 exhibits the largest average surface energy, while the AMPTES sizing showed the lowest. The DGEBA/IPD epoxy experienced the greatest decrease (absolute and percent) due to the presence of absorbed water. Conversely, SiO_2 was least impacted: this statistically insignificant decrease can be attributed to no water being absorbed directly into the SiO_2.

The RDF for a-SiO_2 extracted from the slab composite system was investigated as a function of depth for dry and fully saturated conditions, Supplemental Fig. 3. For the saturated structure, the Si-O peak was wider, while the O-O peak was not as pronounced, consistent with other studies on the effects of water on the a-SiO_2 surface [35]. Interfacial energy comparisons for a-SiO_2 are challenging due to limited literature data at lower temperatures. An experimental interfacial energy of the a-SiO_2 surface is reported to be $(330 \pm 40)\,\mathrm{mJm^{-2}}$ at 2000 K with a temperature coefficient of $-10\,\mathrm{mJm^{-2}}$

per 100 K [36]. Using this, the interfacial energy is extrapolated to be 500 mJm^{-2} at 300 K. This is an order of magnitude larger than (59.79 ± 3.01) mJm^{-2} in this work. However our value is similar to other experimentally-derived interfacial energies, 45 mJm^{-2} in brine at 368 K [37] and 46 mJm^{-2} at 298 K [38]. Interfacial energies for a-SiO_2 nanoparticles of various sizes determined with different molecular dynamics potentials yield wide-ranging values of 100 mJm^{-2} calculated at 350 K [39] and an extrapolated value of 1160 mJm^{-2} at 300 K [40]. The value in the present work is a factor of two smaller than the lowest calculated value, which is attributed to the use of a different interatomic potentials and the assumption of a spherical geometry in determining the interfacial area in [39]. The order of magnitude difference between the other reported values is likely a result of using a linear extrapolation over two orders of magnitude in temperature. For AMPTES, the surface energy finds excellent agreement with a suggested value of 18.08 mJm^{-2} [15].

The work of adhesion at each interface was considered for dry and saturated conditions, Table 2 and Fig. 4. For the dry system, the SiO_2-sizing interface had the largest work of adhesion, while sizing-epoxy was much lower, indicating that sizing-epoxy in the critical interface for failure. The SiO_2-epoxy (unsized) interface shows significantly lower adhesion when compared to the sized system. The work of adhesion for the unsized SiO_2-epoxy interface was calculated as 207.85 mJ m^{-2}, in agreement with contact angle measurements suggesting a range of 178 - 291 mJ m^{-2} for SiO_2-epoxy interfaces [41]. Further, this corresponds closely with a range of 147 - 188 mJ m^{-2} suggested for a simulated SiO_2-epoxy interface [14]. For saturated conditions, the relative adhesion difference between SiO_2-sizing and sizing-epoxy is greatly diminished; however, the sizing-epoxy interface was again found to be the critical system interface.

It is important to note that, in reality, the sizing forms an interpenetrating polymer network with the epoxy [33, 34]. These rather complex network interactions make it difficult to predict precisely where in the interface failure will occur. The simulated slab composite had an idealised geometry, from which failure in both dry and saturated systems is predicted to occur at the sizing-epoxy interface.

Atomic configurations were saved throughout the GCMC saturation process at 0.5, 1.0, and 1.5 wt.% water, allowing W_{12} for each interface as a function of equivalent composite water content to be calculated, Fig. 5. A linear trend is observed for each. The steeper slope of the SiO_2-sizing interface indicates a higher sensitivity to water compared to sizing-epoxy. If these trends were to continue, at some $M_c > 0.99$ wt.%, SiO_2-sizing could become the controlling, critical interface. This could be achieved at T > 300 K and/or P > 1 atm [42]. The work of adhesion for each interface in the

slab composite was further investigated through breaking down the individual energetic contributions at varying water contents, Table 3 and Supplemental Fig. 4. It is clear that non-bonded (van der Waals and Coulombic) and torsional terms make the largest contribution to adhesion. This result agrees with other studies on adhesion at polymer-polymer [13], SiO_2-epoxy [14], and polymer-silane [15] interfaces. In addition to making the largest overall contribution to adhesion, non-bonded terms exhibit the greatest sensitivity to the presence of absorbed water and dominate the loss of adhesive strength. Theoretically, adhesion loss could be significantly minimised through altering the sizing or epoxy systems in a way such that the non-bonded and torsional contributions are retained with increasing composite water content.

3.4. Tensile Testing

Table 4 summarises the tensile testing data for the dry and saturated composite samples. For the dry samples, the average elastic modulus (E), tensile strength (UTS), and strain to failure (ϵ_f) compared well with values of $E = 34.4$ GPa, $UTS = 763$ MPa, and $\epsilon_f = 2.61\%$ suggested for a $[0]_4$ composite with $V_f = 52\%$ using the same [Saertex U14EU920] fibre [43]. The average E of the saturated samples decreased by 14%, UTS showed a 19% decrease, while ϵ_f decreased by 11%. Overall, the saturated samples exhibited noticeable reductions in tensile strength and modulus, with a less significant decrease in strain to failure, aligning well with other studies on the effects of water on the mechanical properties of glass fibre composites [2, 3].

A linear relationship between work of adhesion and tensile strength for silica particle reinforced composites has been reported [44]. Under this assumption and using the fitted linear relationship between work of adhesion and composite water content from Fig. 5, predictions for tensile strength at varying composite water contents were made, Fig. 6. This is equivalent to a linear interpolation between the two experimental values, black markers. These lower water contents would correspond to full saturation for systems exposed to lower humidity, temperature, or pressure.

Figure 7 shows representative images of the failure region for the dry and saturated samples. The thickness of the sizing is sub-micron in scale and is not distinguishable from the more prominent fibre surface and bulk epoxy; therefore, it is difficult to say with certainty if the sizing remains on the surface of the fibre in either case. The dry samples showed substantially more epoxy remaining on the fibre surface, while the saturated samples showed a cleaner fibre surface, in agreement with other studies [45]. This suggests more cohesive failures in the matrix for the dry samples, while the relatively clean fibre surface of the saturated samples indicate a greater tendency for adhesive failures at the interface.

More frequent cohesive epoxy failures for dry samples indicated adhesive failures at the SiO_2-sizing or sizing-epoxy interface occurred more readily for saturated samples. Overall, the SEM results align with the MD predictions, wherein the adhesion at each interface was greatly decreased in saturated conditions. This decrease in adhesion strength makes it seemingly more likely that adhesive interface failure will occur rather than cohesive failures in the bulk epoxy.

4. Conclusions

Ten thermodynamically equivalent slab composite interfaces of DGEBA/IPD epoxy, AMPTES silane sizing, and SiO_2 glass fibre were generated. Simulation procedures for saturating the system based on Grand Canonical Monte Carlo (GCMC) exchanges of noble water molecules were developed. An average solubility limit of 2.07 wt.% water was found corresponding to 0.99 wt.% water in the equivalent full composite, comparing favourably with the experimentally determined 1.15 ± 0.02 wt.% water.

Results for both dry and saturated conditions indicated sizing-epoxy as the critical interface for failure. However, the work of adhesion for SiO_2-sizing is more sensitive to absorbed water. Non-bonded and torsional contributions to the system potential dominated the interface adhesion. Non-bonded contributions were most sensitive to absorbed water and were the primary contributors to adhesion loss for all interfaces.

Results from the SEM analysis further confirmed simulation outputs. After failure, the saturated samples displayed much cleaner fibre surfaces, with far less visibly adhered epoxy. This indicates the saturated samples are more likely to display adhesive interface failures, while dry samples seem to fail more regularly in the bulk epoxy.

The applications of Molecular Dynamics as a tool for better understanding adhesion at the fibre composite interface shows promise, but ultimately requires further development. The simulations considered only a specific, idealised slab composite interface system. Expanding this work to include other epoxy (composition and crosslink density) and fibre sizing systems (composition and wt.% applied) would be beneficial. Furthermore, incorporating polar bonding would introduce complexities to the simulation and could provide better understanding of the effects of water on interfacial adhesion. With further refinement, the methods presented in this work may find more direct applications in the overall design of composite systems.

5. Acknowledgements

MTS was supported by a University of Canterbury College of Engineering PhD scholarship.

6. References

[1] C. Shen, G. Springer, Moisture Absorption and Desorption of Composite Materials, Journal of Composite Materials 10 (1) (1976) 2–20. doi:10.1177/002199837601000101.

[2] C. L. Schutte, Environmental durability of glass-fiber composites, Materials Science and Engineering R: Reports 13 (7) (1994) 265–324.

[3] W. Bradley, T. Grant, The effect of the moisture absorption on the interfacial strength of polymeric matrix composites, Journal of Materials Science 30 (21) (1995) 5537–5542. doi:10.1007/BF00351570.

[4] D. Olmos, R. López-Morón, J. González-Benito, The nature of the glass fibre surface and its effect in the water absorption of glass fibre/epoxy composites. The use of fluorescence to obtain information at the interface, Composites Science and Technology 66 (15) (2006) 2758–2768. doi:10.1016/j.compscitech.2006.03.004.

[5] J. Gonzalez-Benito, The nature of the structural gradient in epoxy curing at a glass fiber/epoxy matrix interface using FTIR imaging, Journal of Colloid and Interface Science 267 (2) (2003) 326–332. doi:10.1016/S0021-9797(03)00550-2.

[6] N. Sharma, M. Surendra Kumar, B. Ray, Study of the effect of hygrothermal ageing on glass/epoxy micro-composites by FTIR-imaging and alternating DSC techniques, Journal of Reinforced Plastics and Composites 27 (15) (2008) 1625–1634. doi:10.1177/0731684407086318.

[7] G. Kotsikos, A. Gibson, J. Mawella, Assessment of moisture absorption in marine GRP laminates with aid of nuclear magnetic resonance imaging, Plastics, Rubber and Composites 36 (9) (2007) 413–418. doi:10.1179/174328907X248203.

[8] S. Chaudhuri, R. Chaudhuri, R. Benner, M. Penugonda, Raman spectroscopy for characterization of interfacial debonds between carbon fibers and polymer matrices, Composite Structures 76 (4) (2006) 375–387. doi:10.1016/j.compstruct.2005.05.009.

[9] A. Zafar, F. Bertocco, J. Schjødt-Thomsen, J. Rauhe, Investigation of the long term effects of moisture on carbon fibre and epoxy matrix composites, Composites Science and Technology 72 (6) (2012) 656–666. doi:10.1016/j.compscitech.2012.01.010.

[10] M. Stoffels, M. Staiger, C. Bishop, Equilibrium moisture content of a crosslinked epoxy network via molecular dynamics simulations, Modelling and Simulation in Materials Science and Engineering 24 (5). doi:10.1088/0965-0393/24/5/055002.

[11] C. Wu, W. Xu, Atomistic molecular modelling of crosslinked epoxy resin, Polymer 47 (16) (2006) 6004–6009. doi:10.1016/j.polymer.2006.06.025.

[12] V. Varshney, S. Patnaik, A. Roy, B. Farmer, A molecular dynamics study of epoxy-based networks: Cross-linking procedure and prediction of molecular and material properties, Macromolecules 41 (18) (2008) 6837–6842. doi:10.1021/ma801153e.

[13] T. Clancy, W. Mattice, Computer simulation of polyolefin interfaces, Computational and Theoretical Polymer Science 9 (3–4) (1999) 261–270. doi:10.1016/S1089-3156(99)00013-6.

[14] O. Holck, E. Dermitzaki, B. Wunderle, J. Bauer, B. Michel, Basic thermo-mechanical property estimation of a 3D-crosslinked epoxy/SiO2 interface using molecular modelling, Microelectronics Reliability 51 (6) (2011) 1027–1034. doi:10.1016/j.microrel.2011.03.014.

[15] M. Deng, V. Tan, T. Tay, Atomistic modeling: Interfacial diffusion and adhesion of polycarbonate and silanes, Polymer 45 (18) (2004) 6399–6407. doi:10.1016/j.polymer.2004.06.055.

[16] J. Thomason, L. Adzima, Sizing up the interphase: An insider's guide to the science of sizing, Composites Part A: Applied Science and Manufacturing 32 (3-4) (2001) 313–321. doi:10.1016/S1359-835X(00)00124-X.

[17] S. Plimpton, Fast parallel algorithms for short-range molecular dynamics, Journal of Computational Physics 117 (1) (1995) 1–19. doi:10.1006/jcph.1995.1039.

[18] W. Hoover, Canonical dynamics: Equilibrium phase-space distributions, Physical Review A 31 (3) (1985) 1695–1697. doi:10.1103/PhysRevA.31.1695.

[19] H. Berendsen, J. Postma, W. Van Gunsteren, A. Dinola, J. Haak, Molecular dynamics with coupling to an external bath, The Journal of Chemical Physics 81 (8) (1984) 3684–3690.

[20] S. Garofalini, A molecular dynamics simulation of the vitreous silica surface, The Journal of Chemical Physics 78 (4) (1983) 2069–2072.

[21] B. Feuston, S. Garofalini, Empirical three-body potential for vitreous silica, The Journal of Chemical Physics 89 (9) (1988) 5818–5824.

[22] B. Brooks, R. Bruccoleri, B. Olafson, D. States, S. Swaminathan, M. Karplus, CHARMM: A program for macromolecular energy, minimization, and dynamics calculations, Journal of Computational Chemistry 4 (2) (1983) 187–217. doi:10.1002/jcc.540040211.

[23] T. Soules, Molecular dynamic calculations of glass structure and diffusion in glass, Journal of Non-Crystalline Solids 49 (1-3) (1982) 29–52. doi:10.1016/0022-3093(82)90107-7.

[24] J. Thomason, P. Jenkins, L. Yang, J. Thomason, P. Jenkins, L. Yang, Glass Fibre Strength—A Review with Relation to Composite Recycling, Fibers 4 (2) (2016) 18. doi:10.3390/fib4020018.

[25] L. Martinez, R. Andrade, E. Birgin, J. Martínez, PACKMOL: A package for building initial configurations for molecular dynamics simulations, Journal of Computational Chemistry 30 (13) (2009) 2157–2164. doi:10.1002/jcc.21224.

[26] T. Okabe, Y. Oya, K. Tanabe, G. Kikugawa, K. Yoshioka, Molecular dynamics simulation of crosslinked epoxy resins: Curing and mechanical properties, European Polymer Journal 80 (2016) 78–88. doi:10.1016/j.eurpolymj.2016.04.019.

[27] W. Jorgensen, J. Chandrasekhar, J. Madura, R. Impey, M. Klein, Comparison of simple potential functions for simulating liquid water, The Journal of Chemical Physics 79 (2) (1983) 926–935.

[28] N. Metropolis, A. Rosenbluth, M. Rosenbluth, A. Teller, E. Teller, Equation of state calculations by fast computing machines, The Journal of Chemical Physics 21 (6) (1953) 1087–1092.

[29] G. Domotor, R. Hentschke, Atomistically modeling the chemical potential of small molecules in dense systems, Journal of Physical Chemistry B 108 (7) (2004) 2413–2417.

[30] ASTM Standard D3039: Standard Test Method for Tensile Properties of Polymer Matrix Composite Materials, ASTM International.

[31] F. Wallenberger, Structural Silicate and Silica Glass Fibers, Advanced Inorganic Fibers Processes, Structures, Properties, Applications (1999) 129–168.

[32] T. Okabe, T. Takehara, K. Inose, N. Hirano, M. Nishikawa, T. Uehara, Curing reaction of epoxy resin composed of mixed base resin and curing agent: Experiments and molecular simulation, Polymer 54 (17) (2013) 4660–4668. doi:10.1016/j.polymer.2013.06.026.

[33] F. Jones, A review of interphase formation and design in fibre-reinforced composites, Journal of Adhesion Science and Technology 24 (1) (2010) 171–202. doi:10.1163/016942409X12579497420609.

[34] X. Liu, J. Thomason, F. Jones, XPS and AFM study of interaction of organosilane and sizing with E-glass fibre surface, Journal of Adhesion 84 (4) (2008) 322–338. doi:10.1080/00218460802004386.

[35] B. Feuston, S. Garofalini, Water-induced relaxation of the vitreous silica surface, Journal of Applied Physics 68 (9) (1990) 4830–4836. doi:10.1063/1.346142.

[36] Book Series: Handbook of Glass Data, https://www.elsevier.com/books/book-series/handbook-of-glass-data.

[37] A. Makrides, M. Turner, J. Slaughter, Condensation of silica from supersaturated silicic acid solutions, Journal of Colloid And Interface Science 73 (2) (1980) 345–367. doi:10.1016/0021-9797(80)90081-8.

[38] G. Alexander, The effect of particle size on the solubility of amorphous silica in water, Journal of Physical Chemistry 61 (11) (1957) 1563–1564.

[39] V. Van Hoang, Molecular dynamics simulation of amorphous SiO2 nanoparticles, Journal of Physical Chemistry B 111 (44) (2007) 12649–12656. doi:10.1021/jp074237u.

[40] A. Roder, W. Kob, K. Binder, Structure and dynamics of amorphous silica surfaces, The Journal of Chemical Physics 114 (17) (2001) 7602–7614. doi:10.1063/1.1360257.

[41] I. Yarovsky, Atomistic simulation of interfaces in materials: Theory and applications, Australian Journal of Physics 50 (2) (1997) 407–424.

[42] T. Tsotsis, S. Keller, K. Lee, J. Bardis, J. Bish, Aging of polymeric composite specimens for 5000 hours at elevated pressure and temperature, Composites Science and Technology 61 (1) (2001) 75–86. doi:10.1016/S0266-3538(00)00196-2.

[43] D. Samborksy, D. Miller, SNL/MSU/DOE Composite Material Fatigue Database 25.0.

[44] S. Shang, J. Williams, K.-J. Söderholm, How the work of adhesion affects the mechanical properties of silica-filled polymer composites, Journal of Materials Science 29 (9) (1994) 2406–2416. doi:10.1007/BF00363434.

[45] J. Iglesias, J. González-Benito, A. Aznar, J. Bravo, J. Baselga, Effect of glass fiber surface treatments on mechanical strength of epoxy based composite materials, Journal of Colloid and Interface Science 250 (1) (2002) 251–260. doi:10.1006/jcis.2002.8332.

7. Figure Captions

Figure 1: MD visualisation of the slab composite interface structure with approximate dimensions, where the x- and z-directions represent the longitudinal and transverse fibre directions, respectively.

Figure 2: The water weight content calculated using a moving 5 Å window, where each point represents the average (over the ten simulated slab composites) wt.% water for the previous 5 Å. The shaded regions represent the average wt.% water in the epoxy (yellow) and the sizing (blue).

Figure 3: The surface energy, γ, for SiO_2, DGEBA-IPD epoxy, and AMPTES sizing under dry and saturated conditions. The error bars indicate standard deviation over the ten equivalent slab composites.

Figure 4: The work of adhesion, W_{12}, for (a) SiO_2-sizing, (b) sizing-epoxy, and (c) SiO_2-epoxy (unsized) interfaces under dry and saturated conditions. The error bars indicate standard deviation over the ten equivalent slab composites.

Figure 5: The work of adhesion for each interface with increasing composite wt.% water. The x-axis is the equivalent composite water content calculated from Eqn. (3). Errors bars indicate standard deviation for the ten equivalent slab composites.

Figure 6: Predicted linear decrease in tensile strength with increasing composite water content. Black circles are experimental strength data and simulated water content.

Figure 7: Scanning electron micrographs of the fracture surface of (a) dry and (b) saturated tensile-tested specimens.

8. Tables

Table 1: Surface energies (mJ m^{-2}) for dry and saturated conditions.

	Dry	Saturated	Change
SiO_2	59.79 ± 3.01	55.11 ± 5.81	-6%
DGEBA/IPD	39.07 ± 2.24	28.28 ± 4.08	-28%
AMPTES	18.28 ± 1.83	14.81 ± 3.74	-20%

Table 2: Work of adhesion (mJ m^{-2}) for dry and saturated conditions for (a) SiO_2-sizing, (b) sizing-epoxy, and (c) SiO_2-epoxy (unsized)

	Dry	Saturated	Change
(a)	392.21 ± 14.23	267.88 ± 21.33	-32%
(b)	252.35 ± 11.30	191.01 ± 26.07	-24%
(c)	207.85 ± 13.07	148.61 ± 22.19	-29%

Table 3: Average contributions to the simulated interface work of adhesion (mJ m^{-2}) for dry and saturated conditions.

	SiO_2 - sizing			**sizing - epoxy**			**SiO_2 - epoxy**		
	Dry	Sat	Change	Dry	Sat	Change	Dry	Sat	Change
Non-bonded	303.48	213.20	-30%	164.10	124.95	-24%	131.05	89.70	-32%
Torsion	131.05	107.08	-18%	89.45	74.56	-17%	53.13	40.58	-23%
Stretching	-27.26	-33.27	-22%	22.96	19.60	-15%	17.92	14.22	-21%
Bending	-15.05	-19.13	-27%	-24.16	-28.10	-16%	5.75	4.11	-29%
Total	392.21	267.88	-32%	252.35	191.01	-24%	207.85	148.61	-29%

Table 4: Tensile properties of dry and saturated $[0]_4$ composite samples.

	E (GPa)	UTS (MPa)	ϵ_f (%)
Dry	30.13 ± 2.21	701.6 ± 36.2	2.33 ± 0.17
Saturated	25.94 ± 1.49	569.4 ± 27.5	2.18 ± 0.34

9. Figures

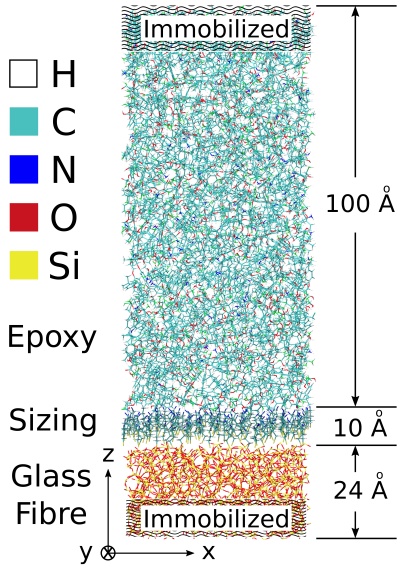

Figure 1: MD visualisation of the slab composite interface structure with approximate dimensions, where the x- and z-directions represent the longitudinal and transverse fibre directions, respectively.

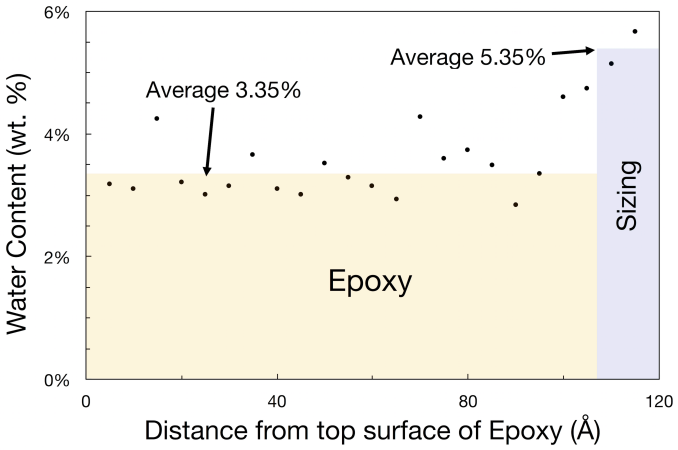

Figure 2: The water weight content calculated using a moving 5 Å window, where each point represents the average (over the ten simulated slab composites) wt.% water for the previous 5 Å. The shaded regions represent the average wt.% water in the epoxy (yellow) and the sizing (blue).

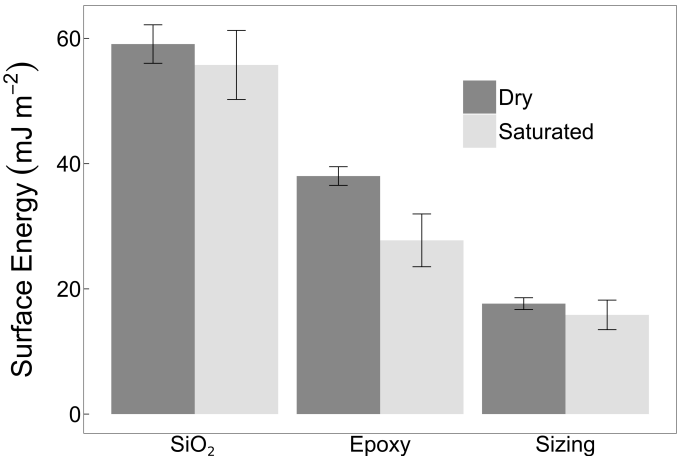

Figure 3: The surface energy, γ, for SiO_2, DGEBA-IPD epoxy, and AMPTES sizing under dry and saturated conditions. The error bars indicate standard deviation over the ten equivalent slab composites.

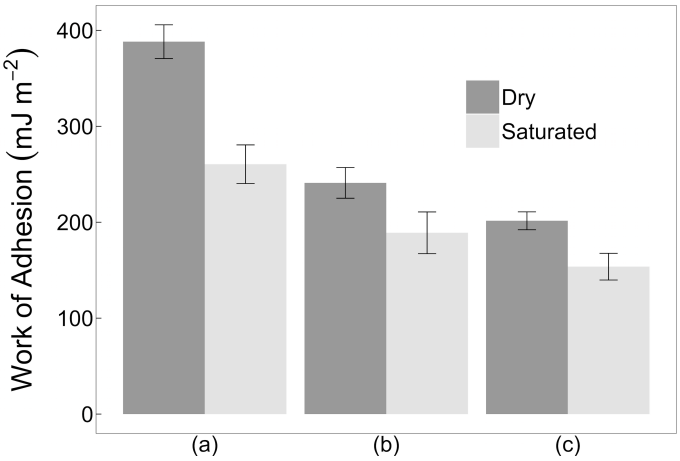

Figure 4: The work of adhesion, W_{12}, for (a) SiO_2-sizing, (b) sizing-epoxy, and (c) SiO_2-epoxy (unsized) interfaces under dry and saturated conditions. The error bars indicate standard deviation over the ten equivalent slab composites.

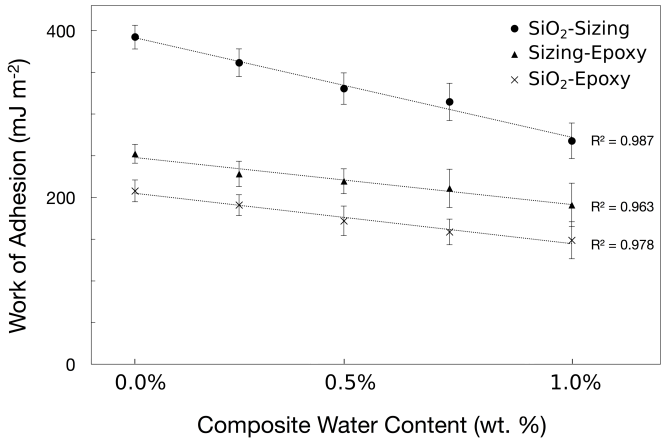

Figure 5: The work of adhesion for each interface with increasing composite wt.% water. The x-axis is the equivalent composite water content calculated from Eqn. (3). Errors bars indicate standard deviation for the ten equivalent slab composites.

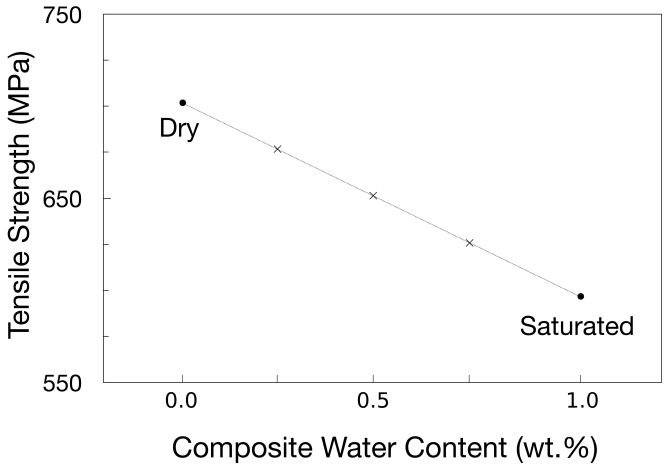

Figure 6: Predicted linear decrease in tensile strength with increasing composite water content. Black circles are experimental strength data and simulated water content.

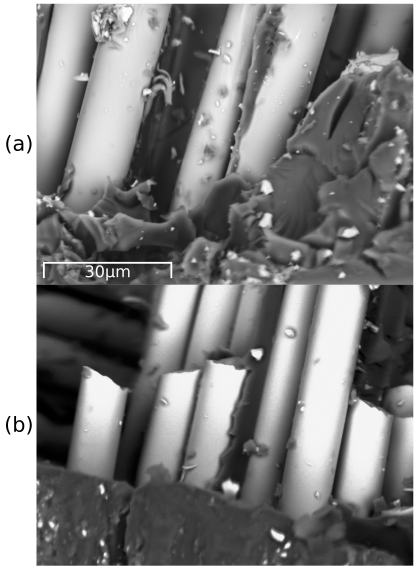

Figure 7: Scanning electron micrographs of the fracture surface of (a) dry and (b) saturated tensile-tested specimens.